

Blind Spatial Signature Estimation via Time-Varying User Power Loading and Parallel Factor Analysis

Yue Rong, *Student Member, IEEE*, Sergiy A. Vorobyov, *Member, IEEE*, Alex B. Gershman, *Senior Member, IEEE*, and Nicholas D. Sidiropoulos, *Senior Member, IEEE*

Abstract—In this paper, the problem of blind spatial signature estimation using the parallel factor (PARAFAC) analysis model is addressed in application to wireless communications. A time-varying user power loading in the uplink mode is proposed to make the model identifiable and to enable application of PARAFAC analysis. Then, identifiability issues are studied in detail and closed-form expressions for the corresponding modified Cramér–Rao bound (CRB) are obtained. Furthermore, two blind spatial signature estimation algorithms are developed. The first technique is based on the PARAFAC fitting trilinear alternating least squares (TALS) regression procedure, whereas the second one makes use of the joint approximate diagonalization algorithm. These techniques do not require any knowledge of the propagation channel and/or sensor array manifold and are applicable to a more general class of scenarios than earlier approaches to blind spatial signature estimation.

Index Terms—Blind spatial signature estimation, parallel factor analysis, sensor array processing.

I. INTRODUCTION

THE USE of antenna arrays at base stations has recently gained much interest due to their ability to combat fading, increase system capacity and coverage, and mitigate interference [1]–[5]. In the uplink communication mode, signals from different users can be separated at the base station antenna array based on the knowledge of their spatial signatures [5]–[8]. In particular, known spatial signatures can be used for beamforming to separate each user of interest from the other (interfering) users. However, user spatial signatures are usually unknown at the base station and, therefore, have to be estimated.

Manuscript received July 21, 2003; revised March 25, 2004. The work of A. B. Gershman was supported by the Wolfgang Paul Award Program of the Alexander von Humboldt Foundation, Germany; the Natural Sciences and Engineering Research Council (NSERC) of Canada; Communications and Information Technology Ontario (CITO); and the Premier’s Research Excellence Award Program of the Ministry of Energy, Science, and Technology (MEST) of Ontario. The work of N. D. Sidiropoulos was supported by the Army Research Laboratory through participation in the ARL Collaborative Technology Alliance (ARL-CTA) for Communications and Networks under Cooperative Agreement DADD19-01-2-0011. The associate editor coordinating the review of this manuscript and approving it for publication was Dr. Constantinos B. Papadias.

Y. Rong and S. A. Vorobyov are with the Department of Communication Systems, University of Duisburg-Essen, Duisburg, 47057 Germany.

A. B. Gershman is with the Department of Communication Systems, University of Duisburg-Essen, Duisburg, 47057 Germany, on leave from the Department of Electrical and Computer Engineering, McMaster University, Hamilton, ON, L8S 4K1 Canada.

N. D. Sidiropoulos is with the Department of Electronic and Computer Engineering, Technical University of Crete, Chania 73100, Greece, and also with the Department of Electrical and Computer Engineering, University of Minnesota, Minneapolis, MN 55455 USA.

Digital Object Identifier 10.1109/TSP.2005.845441

Traditional (nonblind) approaches to spatial signature estimation make use of training sequences that are periodically transmitted by each user and are known at the base station [6]. However, the use of training sequences reduces the information transmission rate, and strict coordination of the training epochs of several users in a multiuser setting requires tight synchronization. As a result, blind spatial signature estimation techniques have attracted significant attention in the literature [8]–[16].

There are several blind approaches to spatial signature estimation. The most common one is based on the parametric modeling of spatial signatures using direction-of-arrival (DOA) parameters [5], [8], [9]. For example, in [5], the coherently distributed source model is used to parameterize the spatial signature. Unfortunately, the source angular spread should be small for the first-order Taylor series expansion used in [5] to be valid. This is a limitation for mobile communications applications in urban environments with low base station antenna mast heights, where angular spreads up to 25° are typically encountered [17], [18]. Furthermore, the approach of [5] requires precise array calibration.

Two other DOA-based blind spatial signature estimation methods are developed in [8] and [9]. In these papers, the source spatial signature is modeled as a plane wave distorted by unknown direction-independent gains and phases. The latter assumption can be quite restrictive in wireless communications where spatial signatures may have an arbitrary form, and therefore, such gains and phases should be modeled as DOA-dependent quantities. As a result, the techniques of [8] and [9] are applicable to a particular class of scenarios only.

Another popular approach to blind spatial signature estimation makes use of the cyclostationary nature of communication signals [10], [11]. This approach does not make use of any DOA-based model of spatial signatures, but it is applicable only to users that all have different cyclic frequencies. The latter condition implies that the users must have different carrier frequencies [which is not the case for Space-Division Multiple Access (SDMA)] and/or baud rates [11]. This can limit practical applications of the methods of [10] and [11].

One more well-developed approach to this problem employs higher order statistics (cumulants) to estimate spatial signatures in a blind way [12]–[16]. Cumulant-based methods are only applicable to non-Gaussian signals. Moreover, all such algorithms are restricted by the requirement of a large number of snapshots. This requirement is caused by a slow convergence of sample estimates of higher order cumulants.

The aforementioned restrictions of cumulant-based methods have been a strong motivation for further attempts to develop

blind spatial signature estimators that are based on second-order statistics only and do not require any DOA-related or cyclostationarity assumptions. In [15], such a method was proposed using joint approximate diagonalization of a set of spatial auto- and cross-covariance matrices. This method requires an existence of a long-time coherence of the source signals to obtain enough cross-covariance matrices at multiple lags for the joint diagonalization process and to guarantee identifiability. In practical wireless communication systems, the signal time coherence is severely limited, i.e., the correlation time of the received signals typically does not largely exceed the sampling interval. For example, communication signals sampled at the symbol rate are uncorrelated,¹ and hence, higher lag correlations are all zero. In such cases, multiple covariance matrices are unavailable, and the method of [15] is not applicable. Furthermore, [15] offers limited identifiability—for example, it requires that the matrix of spatial signatures be full column rank, and therefore, the number of sources should be less or equal to the number of antennas.

In this paper, we develop a new bandwidth-efficient approach to blind spatial signature estimation using PARAFAC analysis [20]–[23]. Our approach does not require any restrictive assumptions on the array geometry and the propagation environment. Time-varying user power loading is exploited to obtain multiple spatial zero-lag covariance matrices required for the PARAFAC model.

Blind PARAFAC multisensor reception and spatial signature estimation have been considered earlier in [21] and [23]. However, the approach of [21] is applicable to direct sequence-code division multiple access (DS-CDMA) systems only, as spreading is explicitly used as the third dimension of the data array, whereas [23] requires multiple shifted but otherwise identical subarrays and a DOA parameterization. Below, we show that the proposed user power loading enables us to give up the CDMA and multiple-invariance/DOA parameterization assumptions and extend the blind approach to any type of SDMA system employing multiple antennas at the receiver.

Blind source separation of nonstationary sources using multiple covariance matrices has also been considered in [24] but, again, under limited identifiability conditions, stemming from the usual ESPRIT-like solution. Our identifiability results are considerably more general as they do not rely on this limited viewpoint.

The rest of this paper is organized as follows. The signal model is introduced in Section II. Section III formulates the spatial signature estimation problem in terms of three-way analysis using time-varying user power loading. The identifiability of this model is studied in Section IV. Two spatial signature estimators are presented in Section V: PARAFAC fitting based on the trilinear alternating least squares (TALS) regression procedure and a joint approximate diagonalization-based estimator. A modified deterministic CRB for the problem at hand is derived in Section VI. Simulation results are presented in Section VII. Conclusions are drawn in Section VIII.

¹Channel-coded signals, which include redundancy for error correction, are in fact interleaved before transmission, with the goal of making the transmitted signal approximately uncorrelated.

II. DATA MODEL

Let an array of K sensors receive the signals from M narrowband sources. We assume that the observation interval is shorter than the coherence time of the channel (i.e., the scenario is time-invariant), and the time dispersion introduced by the multipath propagation is small in comparison with the reciprocal of the bandwidth of the emitted signals [5]. Under such assumptions, the $K \times 1$ snapshot vector of antenna array outputs can be written as [5]

$$\mathbf{y}(n) = \mathbf{A}\mathbf{s}(n) + \mathbf{v}(n) \quad (1)$$

where $\mathbf{A} = [\mathbf{a}_1, \dots, \mathbf{a}_M] \in \mathbb{C}^{K \times M}$ is the matrix of the user spatial signatures, $\mathbf{a}_m = [a_{1,m}, \dots, a_{K,m}]^T \in \mathbb{C}^{K \times 1}$ is the spatial signature of the m th user, $\mathbf{s}(n) = [s_1(n), \dots, s_M(n)]^T \in \mathbb{C}^{M \times 1}$ is the vector of the equivalent baseband user waveforms, $\mathbf{v}(n) = [v_1(n), \dots, v_K(n)]^T \in \mathbb{C}^{K \times 1}$ is the vector of additive spatially and temporally white Gaussian noise, and $(\cdot)^T$ denotes the transpose. Note that in contrast to direction finding problems, the matrix \mathbf{A} is unstructured. Assuming that there is a block of N snapshots available, the model (1) can be written as

$$\mathbf{Y} = \mathbf{A}\mathbf{S} + \mathbf{V} \quad (2)$$

where $\mathbf{Y} = [\mathbf{y}(1), \dots, \mathbf{y}(N)] \in \mathbb{C}^{K \times N}$ is the array data matrix, $\mathbf{S} = [\mathbf{s}(1), \dots, \mathbf{s}(N)] \in \mathbb{C}^{M \times N}$ is the user waveform matrix, and $\mathbf{V} = [\mathbf{v}(1), \dots, \mathbf{v}(N)] \in \mathbb{C}^{K \times N}$ is the sensor noise matrix. A quasistatic channel is assumed throughout the paper. This assumption means that the spatial signatures are block time-invariant (i.e., the elements of \mathbf{A} remain constant over a block of N snapshots).

Assuming that the user signals are uncorrelated with each other and sensor noise, the array covariance matrix of the received signals can be written as

$$\mathbf{R} \triangleq \mathbb{E} \{ \mathbf{y}(n) \mathbf{y}^H(n) \} = \mathbf{A}\mathbf{Q}\mathbf{A}^H + \sigma^2 \mathbf{I} \quad (3)$$

where $\mathbf{Q} \triangleq \mathbb{E} \{ \mathbf{s}(n) \mathbf{s}^H(n) \}$ is the diagonal covariance matrix of the signal waveforms, σ^2 is the sensor noise variance, \mathbf{I} is the identity matrix, and $(\cdot)^H$ denotes the Hermitian transpose.

The problem studied in this paper is the estimation of the matrix \mathbf{A} from noisy array observations \mathbf{Y} .

III. PARAFAC MODEL

Before proceeding, we need to clarify that by *identifiability*, we mean the uniqueness (up to inherently unresolvable source permutation and scale ambiguities) of all user spatial signatures given the exact covariance data. Identifiability in this sense is impossible to achieve with only one known covariance matrix (3) because the matrix \mathbf{A} can be estimated from \mathbf{R} only up to an arbitrary unknown unitary matrix [22]. The approach we will use to provide a unique user spatial signature estimation is based on an artificial user power loading and PARAFAC model analysis. Therefore, next, we explain how this model is related to our problem.

Let us divide uniformly the whole data block of N snapshots into P subblocks so that each subblock contains $N_s = \lfloor N/P \rfloor$

snapshots, where $\lfloor x \rfloor$ denotes the largest integer less than x . We fix the transmit power of each user within each subblock while changing it artificially² between different subblocks. It should be stressed that the proposed artificial time-varying user power loading does not require precise synchronization among the users, but the users should roughly know the boundaries of epochs over which the powers are kept constant (this can be achieved, for example, using the standard power control feedback channel). Therefore, a certain level of user coordination is required from the transmitter side.³ We stress that the proposed user power loading can be easily implemented by overlaying a small power variation on top of the usual power control, without any other modifications to existing hardware or communication system/network parameters. In addition, as it will be seen in the sequel, the user powers need not vary much to enable blind identification. In particular, power variations that will be used are on the order of 30%. Such power variations will not significantly affect the bit error rate (BER), which is seriously affected only when order-of-magnitude power variations are encountered.

If power control is fast enough (in the sense that there are several power changes per channel coherence dwell), we can exploit it as a sort of user power loading. However, power control is usually much slower than the channel coherence time, because its purpose is to combat long-term shadowing. For this reason, in practice, it may not be possible to rely on the power control variations, and we need to induce a faster (but much smaller in magnitude) power variation on top of power control. This extra power variation need not “follow the channel”, i.e., it can be pseudo-random, and hence, the channel need not be measured any faster than required for regular power control.

Using the proposed power loading, the received snapshots within any p th subblock correspond to the following covariance matrix:

$$\mathbf{R}(p) = \mathbf{A}\mathbf{Q}(p)\mathbf{A}^H + \sigma^2\mathbf{I} \quad (4)$$

where $\mathbf{Q}(p)$ is the diagonal covariance matrix of the user waveforms in the p th subblock. Using all P subblocks, we will have P different covariance matrices $\{\mathbf{R}(1), \dots, \mathbf{R}(P)\}$. Note that these matrices differ from each other only because the signal waveform covariance matrices $\mathbf{Q}(p)$ differ from one subblock to another.

In practice, the noise power can be estimated and then subtracted from the covariance matrix (4). Let us stack the P matrices $\mathbf{R}(p) - \sigma^2\mathbf{I}$, $p = 1, \dots, P$ together to form a three-way array $\underline{\mathbf{R}}$, which is natural to call the *covariance array*. The (i, l, p) th element of such an array can be written as

$$r_{i,l,p} \triangleq [\underline{\mathbf{R}}]_{i,l,p} = \sum_{m=1}^M a_{i,m} \nu_m(p) a_{l,m}^* \quad (5)$$

²Note that the effect of time-varying user powers has been exploited in [24], where an ESPRIT-type algorithm has been proposed for blind source separation of nonstationary sources. Similar ideas have been used in [15] and [25]. However, the authors of [15], [24], and [25] assume that the source powers vary because of signal nonstationarity rather than artificial power loading.

³As it will be seen from our simulations, the methods proposed in the present paper will work well, even in the case when there is no user coordination (i.e., in the unsynchronized user case).

where $\nu_m(p) \triangleq [\mathbf{Q}(p)]_{m,m}$ is the power of the m th user in the p th subblock, and $(\cdot)^*$ denotes the complex conjugate. Defining the matrix $\mathbf{P} \in \mathbb{R}^{P \times M}$ as

$$\mathbf{P} \triangleq \begin{bmatrix} \nu_1(1) & \dots & \nu_M(1) \\ \vdots & \ddots & \vdots \\ \nu_1(P) & \dots & \nu_M(P) \end{bmatrix} \quad (6)$$

we can write the following relationship between $\mathbf{Q}(p)$ and \mathbf{P} :

$$\mathbf{Q}(p) = \mathcal{D}_p\{\mathbf{P}\} \quad (7)$$

for all $p = 1, \dots, P$. In (7), $\mathcal{D}_p\{\cdot\}$ is the operator that makes a diagonal matrix by selecting the p th row and putting it on the main diagonal while putting zeros elsewhere.

Equation (5) implies that $r_{i,l,p}$ is a sum of rank-1 triple products. If M is sufficiently small,⁴ (5) represents a low-rank decomposition of $\underline{\mathbf{R}}$. Therefore, the problem of spatial signature estimation can be reformulated as the problem of low-rank decomposition of the three-way covariance array $\underline{\mathbf{R}}$.

IV. PARAFAC MODEL IDENTIFIABILITY

In this section, we study identifiability of the PARAFAC model-based spatial signature estimation. Toward this end, we discuss conditions under which the trilinear decomposition of $\underline{\mathbf{R}}$ is unique. Identifiability conditions on the number of subblocks and the number of array sensors are derived.

We start with the definition of the *Kruskal rank* of a matrix [20].

Definition: The Kruskal rank (or k -rank) of a matrix \mathbf{C} is $k_{\mathbf{C}}$ if and only if every $k_{\mathbf{C}}$ columns of \mathbf{C} are linearly independent and either \mathbf{C} has $k_{\mathbf{C}}$ columns or \mathbf{C} contains a set of $k_{\mathbf{C}} + 1$ linearly dependent columns. Note that k -rank is always less than or equal to the conventional matrix rank. It can be easily checked that if \mathbf{C} is full column rank, then it is also full k rank.

Using (7) and assuming that the noise term is subtracted from the matrix $\mathbf{R}(p)$, we can rewrite (4) as

$$\mathbf{R}(p) = \mathbf{A}\mathcal{D}_p(\mathbf{P})\mathbf{A}^H \quad (8)$$

for all $p = 1, \dots, P$. Let us introduce the matrix

$$\begin{aligned} \mathbf{R}_a &\triangleq \begin{bmatrix} \mathbf{A}\mathcal{D}_1(\mathbf{P})\mathbf{A}^H \\ \mathbf{A}\mathcal{D}_2(\mathbf{P})\mathbf{A}^H \\ \vdots \\ \mathbf{A}\mathcal{D}_P(\mathbf{P})\mathbf{A}^H \end{bmatrix} \\ &= \begin{bmatrix} \mathbf{A}\mathcal{D}_1(\mathbf{P}) \\ \mathbf{A}\mathcal{D}_2(\mathbf{P}) \\ \vdots \\ \mathbf{A}\mathcal{D}_P(\mathbf{P}) \end{bmatrix} \mathbf{A}^H \\ &= (\mathbf{P} \odot \mathbf{A})\mathbf{A}^H \end{aligned} \quad (9)$$

where \odot is the Khatri–Rao (column-wise Kronecker) matrix product [23].

To establish identifiability, we have to obtain under which conditions the decomposition (9) of the matrix \mathbf{R}_a via matrices \mathbf{P} and \mathbf{A} is unique (up to the scaling and permutation ambiguities). In [20], the uniqueness of trilinear decomposition for

⁴Exact conditions for M are given in the next section.

the case of real-valued arrays has been established. These results have been later extended to the complex-valued matrix case [21]. In the context of our present application, which involves a conjugate-symmetric PARAFAC model, the results of [20] and [21] specialize to the following Theorem (see also [28] for a discussion of the corresponding real-symmetric model).

Theorem 1: Consider the set of matrices (8). If for $M > 1$

$$k_{\mathbf{A}} + k_{\mathbf{P}} + k_{\mathbf{A}^*} = 2k_{\mathbf{A}} + k_{\mathbf{P}} \geq 2M + 2 \quad (10)$$

then \mathbf{A} and \mathbf{P} are unique up to inherently unresolvable permutation and scaling of columns, i.e., if there exists any other pair $\{\bar{\mathbf{A}}, \bar{\mathbf{P}}\}$ that satisfies (10), then this pair is related to the pair $\{\mathbf{A}, \mathbf{P}\}$ via

$$\bar{\mathbf{A}} = \mathbf{A}\mathbf{\Pi}\mathbf{\Delta}_1, \quad \bar{\mathbf{P}} = \mathbf{P}\mathbf{\Pi}\mathbf{\Delta}_2 \quad (11)$$

where $\mathbf{\Pi}$ is a permutation matrix, and $\mathbf{\Delta}_1$ and $\mathbf{\Delta}_2$ are diagonal scaling matrices satisfying

$$\mathbf{\Delta}_1\mathbf{\Delta}_1^*\mathbf{\Delta}_2 = \mathbf{I}. \quad (12)$$

For $M = 1$, \mathbf{A} and \mathbf{P} are always unique, irrespective of (10). ■

Note that the scaling ambiguity can be easily avoided by taking one of the array sensors as a reference and normalizing user spatial signatures with respect to it. The permutation ambiguity is unremovable, but it is usually immaterial because typically, the ordering of the estimated spatial signatures is unimportant.

It is worth noting that condition (10) is sufficient for identifiability and is necessary only if $M = 2$ or $M = 3$ but is not necessary if $M \geq 4$ [27]. Furthermore, for $M > 1$, the condition $k_{\mathbf{P}} \geq 2$ becomes necessary [26]. In terms of the number of subblocks, the latter condition requires that

$$P \geq 2. \quad (13)$$

The practical conclusion is that in the multiuser case, not less than two covariance matrices must be collected to uniquely identify \mathbf{A} , which means that the users have to change their powers at least once during the transmission. Similarly, it is necessary that $K > 1$.

The following result gives sufficient conditions for the number of sensors to guarantee almost sure identifiability.⁵

Theorem 2: Suppose the following.

- The elements of \mathbf{A} are drawn from distribution $P_{\mathcal{L}}(\mathbb{C}^{KM})$, which is assumed continuous with respect to the Lebesgue measure in \mathbb{C}^{KM} .
- The elements of \mathbf{P} are drawn from distribution $P_{\mathcal{L}}(\mathbb{R}^{PM})$, which is assumed continuous with respect to the Lebesgue measure in \mathbb{R}^{PM} .

Then, we have the following.

- For $1 < M \leq P$, the value of

$$K \geq \frac{M+2}{2} \quad (14)$$

is sufficient for almost sure identifiability.

⁵The definition of almost sure identifiability in the context discussed is given in [29].

- For $M > P$ and $P \geq 2$, the value of

$$K \geq \frac{2M+2-P}{2} \quad (15)$$

is sufficient for almost sure identifiability.

Proof: The assumptions of Theorem 2 mean that the following equalities hold almost surely [29]:

$$k_{\mathbf{A}} = \text{rank}\{\mathbf{A}\} = \min(K, M) \quad (16)$$

$$k_{\mathbf{P}} = \text{rank}\{\mathbf{P}\} = \min(P, M). \quad (17)$$

Substituting (16) and (17) into (10), we have

$$2\min(K, M) + \min(P, M) \geq 2M + 2. \quad (18)$$

The following cases should be considered:

- 1) $K \geq M$. In this case, $k_{\mathbf{A}} = M$. Furthermore, as $P \geq 2$, we have that $k_{\mathbf{P}} \geq 2$. Therefore, (18) is always satisfied.
- 2) $K < M$; $M \leq P$. In this case, $k_{\mathbf{A}} = K$, $k_{\mathbf{P}} = M$, and (18) becomes

$$2K + M \geq 2M + 2. \quad (19)$$

This inequality is equivalent to (14).

- 3) $K < M$; $M > P$. In this case, $k_{\mathbf{A}} = K$, $k_{\mathbf{P}} = P$, and (18) can be written as

$$2K + P \geq 2M + 2. \quad (20)$$

This inequality is equivalent to (15). ■

V. ESTIMATORS

We will now develop two techniques for blind spatial signature estimation based on the PARAFAC model of Section III.

In practice, the exact covariance matrices $\hat{\mathbf{R}}(p)$ are unavailable but can be estimated from the array snapshots $\mathbf{y}(n)$, $n = 1, \dots, N$. The sample covariance matrices are given by

$$\hat{\mathbf{R}}(p) = \frac{1}{N_s} \sum_{n=(p-1)N_s+1}^{pN_s} \mathbf{y}(n)\mathbf{y}^H(n), \quad p = 1, \dots, P. \quad (21)$$

These matrices can be used to form a sample three-way covariance array denoted as $\hat{\mathbf{R}}$.

If $K > M$, then the noise power σ^2 can be estimated as the average of the smallest $K - M$ eigenvalues of the matrix

$$\tilde{\mathbf{R}} = \frac{1}{P} \sum_{p=1}^P \hat{\mathbf{R}}(p) = \frac{1}{N} \sum_{n=1}^N \mathbf{y}(n)\mathbf{y}^H(n) \quad (22)$$

and the estimated noise component $\hat{\sigma}^2\mathbf{I}$ can be subtracted from subblocks of the sample covariance array $\hat{\mathbf{R}}$. In case $K \leq M$, noise power can be estimated on system start-up before any transmission begins.

To formulate our techniques, we will need ‘‘slices’’ of the matrices $\hat{\mathbf{R}}$ and $\tilde{\mathbf{R}}$ along different dimensions [21]. Toward this end, let us define the ‘‘slice’’ matrices as

$$\mathbf{R}_a^{(i)} \triangleq [r_{i,:,:}] \quad (23)$$

$$\mathbf{R}_b^{(l)} \triangleq [r_{:,l,:}] \quad (24)$$

$$\mathbf{R}_c^{(p)} \triangleq [r_{:,:,p}] \quad (25)$$

where $i, l = 1, \dots, K$; $p = 1, \dots, P$; and $r_{i,l,p} \triangleq [\underline{\mathbf{R}}]_{i,l,p}$. Similarly

$$\hat{\mathbf{R}}_a^{(i)} \triangleq [\hat{r}_{i,:,:}] \quad (26)$$

$$\hat{\mathbf{R}}_b^{(l)} \triangleq [\hat{r}_{:,l,:}] \quad (27)$$

$$\hat{\mathbf{R}}_c^{(p)} \triangleq [\hat{r}_{:,:p}] \quad (28)$$

where $i, l = 1, \dots, K$; $p = 1, \dots, P$; and $\hat{r}_{i,l,p} \triangleq [\hat{\underline{\mathbf{R}}}]_{i,l,p}$.

For the sake of convenience, let us introduce $\mathbf{B} \triangleq \mathbf{A}^H$ and rewrite (9) as

$$\mathbf{R}_a = \begin{bmatrix} \mathbf{R}_a^{(1)} \\ \mathbf{R}_a^{(2)} \\ \vdots \\ \mathbf{R}_a^{(K)} \end{bmatrix} = (\mathbf{P} \odot \mathbf{A})\mathbf{B}. \quad (29)$$

In the same way, let us define the matrices

$$\mathbf{R}_b \triangleq \begin{bmatrix} \mathbf{R}_b^{(1)} \\ \mathbf{R}_b^{(2)} \\ \vdots \\ \mathbf{R}_b^{(K)} \end{bmatrix} = (\mathbf{B}^T \odot \mathbf{P})\mathbf{A}^T \quad (30)$$

$$\mathbf{R}_c \triangleq \begin{bmatrix} \mathbf{R}_c^{(1)} \\ \mathbf{R}_c^{(2)} \\ \vdots \\ \mathbf{R}_c^{(P)} \end{bmatrix} = (\mathbf{A} \odot \mathbf{B}^T)\mathbf{P}^T \quad (31)$$

and their sample estimates

$$\hat{\mathbf{R}}_a \triangleq \begin{bmatrix} \hat{\mathbf{R}}_a^{(1)} \\ \hat{\mathbf{R}}_a^{(2)} \\ \vdots \\ \hat{\mathbf{R}}_a^{(K)} \end{bmatrix}, \quad \hat{\mathbf{R}}_b \triangleq \begin{bmatrix} \hat{\mathbf{R}}_b^{(1)} \\ \hat{\mathbf{R}}_b^{(2)} \\ \vdots \\ \hat{\mathbf{R}}_b^{(K)} \end{bmatrix}, \quad \hat{\mathbf{R}}_c \triangleq \begin{bmatrix} \hat{\mathbf{R}}_c^{(1)} \\ \hat{\mathbf{R}}_c^{(2)} \\ \vdots \\ \hat{\mathbf{R}}_c^{(P)} \end{bmatrix}. \quad (32)$$

Note that for the sake of algorithm simplicity, we will not exploit the fact that our PARAFAC model is symmetric. For example, the algorithm that follows in the next subsection treats \mathbf{A} and \mathbf{B} as independent variables; symmetry will only be exploited in the calculation of the final estimate of \mathbf{A} .

A. TALS Estimator

The basic idea behind the TALS procedure for PARAFAC fitting is to update each time a subset of parameters using LS regression while keeping the previously obtained estimates of the rest of parameters fixed. This alternating projections-type procedure is iterated for all subsets of parameters until convergence is achieved [19], [21], [23], [30].

In application to our problem, the PARAFAC TALS procedure can be formulated as follows.

- **Step 1:** Initialize \mathbf{P} and \mathbf{A} .
- **Step 2:** Find the estimate of \mathbf{B} by solving the following LS problem:

$$\hat{\mathbf{B}} = \arg \min_{\mathbf{B}} \left\| \hat{\mathbf{R}}_a - (\mathbf{P} \odot \mathbf{A})\mathbf{B} \right\|_F^2 \quad (33)$$

whose analytic solution is given by

$$\hat{\mathbf{B}} = (\mathbf{P} \odot \mathbf{A})^\dagger \hat{\mathbf{R}}_a \quad (34)$$

where $(\cdot)^\dagger$ denotes the matrix pseudoinverse. Set $\mathbf{B} = \hat{\mathbf{B}}$.

- **Step 3:** Find the estimate of \mathbf{A} by solving the following LS problem:

$$\hat{\mathbf{A}} = \arg \min_{\mathbf{A}} \left\| \hat{\mathbf{R}}_b - (\mathbf{B}^T \odot \mathbf{P})\mathbf{A}^T \right\|_F^2 \quad (35)$$

whose analytic solution is given by

$$\hat{\mathbf{A}} = \hat{\mathbf{R}}_b^T \left((\mathbf{B}^T \odot \mathbf{P})^\dagger \right)^T. \quad (36)$$

Set $\mathbf{A} = \hat{\mathbf{A}}$.

- **Step 4:** Find the estimate of \mathbf{P} by solving the following LS problem:

$$\hat{\mathbf{P}} = \arg \min_{\mathbf{P}} \left\| \hat{\mathbf{R}}_c - (\mathbf{A} \odot \mathbf{B}^T)\mathbf{P}^T \right\|_F^2 \quad (37)$$

whose analytic solution is given by

$$\hat{\mathbf{P}} = \hat{\mathbf{R}}_c^T \left((\mathbf{A} \odot \mathbf{B}^T)^\dagger \right)^T. \quad (38)$$

Set $\mathbf{P} = \hat{\mathbf{P}}$.

- **Step 5:** Repeat steps 2–4 until convergence is achieved, and then compute the final estimate of \mathbf{A} as $\hat{\mathbf{A}} = (\mathbf{A} + \mathbf{B}^H)/2$.

The complexity of the TALS algorithm is $\mathcal{O}(M^3 + K^2MP)$ per iteration. It is worth noting that when M is small relative to K and P , only a few iterations of this algorithm are usually required to achieve convergence [23].

B. Joint Diagonalization-Based Estimator

Using the idea of [15], we can obtain the estimate of \mathbf{A} by means of a joint diagonalizer of the matrices $\mathbf{R}(p)$, $p = 1, \dots, P$.

The estimator can be formulated as the following sequence of steps:

- **Step 1:** Calculate the eigendecomposition of $\tilde{\mathbf{R}}$, and find the estimate $\hat{\sigma}^2$ of the noise power as the average of the $K - M$ smallest eigenvalues of this matrix.
- **Step 2:** Compute the whitening matrix as

$$\mathbf{W} = \left[(\lambda_1 - \hat{\sigma}^2)^{-\frac{1}{2}} \mathbf{g}_1, \dots, (\lambda_M - \hat{\sigma}^2)^{-\frac{1}{2}} \mathbf{g}_M \right]^H \quad (39)$$

where $\{\lambda_m\}_{m=1}^M$ are the largest (signal-subspace) eigenvalues of $\tilde{\mathbf{R}}$, and $\{\mathbf{g}_m\}_{m=1}^M$ are the corresponding eigenvectors.

- **Step 3:** Compute the prewhitened sample covariance matrices as

$$\hat{\mathbf{C}}(p) = \mathbf{W} \hat{\mathbf{R}}(p) \mathbf{W}^H, \quad p = 1, \dots, P. \quad (40)$$

- **Step 4:** Obtain a unitary matrix \mathbf{U} as a joint diagonalizer of the set of matrices $\{\hat{\mathbf{C}}(p)\}_{p=1}^P$.
- **Step 5:** Estimate the matrix $\hat{\mathbf{A}}$ as

$$\hat{\mathbf{A}} = \mathbf{W}^\dagger \mathbf{U}. \quad (41)$$

Several efficient joint diagonalization algorithms can be used in Step 4; see [31] and [32]. For example, the complexity of the ac-dc algorithm of [32] is $\mathcal{O}(K^2MP + K^3)$ per iteration.

It should be pointed out that the joint diagonalization-based estimator requires stronger conditions in terms of the number of sensors as compared to the TALS estimator. Indeed, $K \geq M$ is required for the joint diagonalization algorithms [15] and [32], whereas this constraint is not needed for TALS.

Both the TALS and joint diagonalization algorithms can be initialized randomly [23]. Alternatively, if power control is fast enough (in the sense that there are several power changes per channel coherence dwell), we can use the fact that the power changes are known at the base station to initialize the matrix \mathbf{P} in TALS. However, as mentioned in Section III, power control algorithms are usually much slower than the channel coherence time because their purpose is to combat long-term shadowing. For this reason, such an initialization of \mathbf{P} may not be possible.

VI. MODIFIED CRAMÉR–RAO BOUND

In this section, we present a modified deterministic CRB on estimating the user spatial signatures.⁶ The model (1) for the n th sample of the p th subblock can be rewritten as

$$\mathbf{y}(p, n) = \mathbf{A}\mathbf{Q}^{\frac{1}{2}}(p)\tilde{\mathbf{s}}(n) + \mathbf{v}(n), \quad n = (p-1)N_s + 1 \dots pn_s \quad (42)$$

where

$$\begin{aligned} \tilde{\mathbf{s}}(n) &\triangleq [\tilde{s}_1(n), \dots, \tilde{s}_M(n)]^T \\ &= \mathbf{Q}^{-\frac{1}{2}}(p)\mathbf{s}(n) \end{aligned} \quad (43)$$

is the vector of normalized signal waveforms, and the normalization is done so that all waveforms have unit powers.

Hence, the observations in the p th subblock satisfy the following model:

$$\mathbf{y}(p, n) \sim \mathcal{CN}(\boldsymbol{\mu}(p, n), \sigma^2 \mathbf{I}) \quad (44)$$

where

$$\boldsymbol{\mu}(p, n) = \mathbf{A}\mathbf{Q}^{\frac{1}{2}}(p)\tilde{\mathbf{s}}(n), \quad n = (p-1)N_s + 1, \dots, pn_s. \quad (45)$$

The unknown parameters of the model (42) are all entries of \mathbf{A} , diagonal elements of $\mathbf{Q}(p)$ ($p = 1, \dots, P$), and the noise power σ^2 . Note that to make the model (42) identifiable, we assume that the signal waveforms are known. Therefore, we study a modified (optimistic) CRB. However, as follows from

⁶The deterministic CRB is a relevant bound in cases when the signal waveforms are unknown deterministic or random with unknown statistics; see, e.g., [33] and [34].

our simulation results in the next section, the performance of the proposed estimators is rather close to this optimistic CRB, and therefore, this bound is relevant.

In addition, note that the parameter σ^2 is decoupled with other parameters in the Fisher information matrix (FIM) [34]. Therefore, without loss of generality, σ^2 can be excluded from the vector of unknown parameters.

A delicate point regarding the CRB for model (42) is the inherent permutation and scaling ambiguities. To get around the problem of scaling ambiguity, we assume that each spatial signature vector is normalized so that its first element is equal to one (after such a normalization the first row of \mathbf{A} becomes $[1, \dots, 1]$). To avoid the permutation ambiguity, we assume that the first row of \mathbf{P} is known and consists of distinct elements. Then, the vector of the parameters of interest can be written as

$$\boldsymbol{\alpha} = [\boldsymbol{\alpha}_2^T, \dots, \boldsymbol{\alpha}_K^T]^T \in \mathbb{R}^{2(K-1)M \times 1} \quad (46)$$

where

$$\boldsymbol{\alpha}_k \triangleq [\text{Re}\{\tilde{\mathbf{a}}_k\}^T, \text{Im}\{\tilde{\mathbf{a}}_k\}^T]^T, \quad \tilde{\mathbf{a}}_k \triangleq [a_{k,1}, \dots, a_{k,M}]^T. \quad (47)$$

The vector of nuisance parameters can be expressed as

$$\boldsymbol{\zeta} = [\tilde{\mathbf{p}}(2), \dots, \tilde{\mathbf{p}}(P)]^T \in \mathbb{R}^{(P-1)M \times 1} \quad (48)$$

where $\tilde{\mathbf{p}}(p)$ is the p th row of the matrix \mathbf{P} .

Using (46) and (48), the vector of unknown parameters can be written as

$$\boldsymbol{\theta} = [\boldsymbol{\alpha}^T, \boldsymbol{\zeta}^T]^T \in \mathbb{R}^{(2(K-1)M + (P-1)M) \times 1}. \quad (49)$$

Theorem 3: The $(2(K-1)M + (P-1)M) \times (2(K-1)M + (P-1)M)$ Fisher Information Matrix (FIM) is given by (50), shown at the bottom of the page, where

$$\begin{aligned} \mathbf{J}_{\boldsymbol{\alpha}_2, \boldsymbol{\alpha}_2} &= \dots = \mathbf{J}_{\boldsymbol{\alpha}_K, \boldsymbol{\alpha}_K} \\ &= \frac{2}{\sigma^2} \begin{bmatrix} \text{Re}\{\boldsymbol{\Upsilon}^H \boldsymbol{\Upsilon}\} & -\text{Im}\{\boldsymbol{\Upsilon}^H \boldsymbol{\Upsilon}\} \\ \text{Im}\{\boldsymbol{\Upsilon}^H \boldsymbol{\Upsilon}\} & \text{Re}\{\boldsymbol{\Upsilon}^H \boldsymbol{\Upsilon}\} \end{bmatrix} \end{aligned} \quad (51)$$

$$\mathbf{J}_{\tilde{\mathbf{p}}(p), \tilde{\mathbf{p}}(p)} = \frac{2}{\sigma^2} \text{Re}\left\{(\mathbf{G}(p))^H \mathbf{G}(p)\right\} \quad (52)$$

$$\mathbf{J}_{\boldsymbol{\alpha}, \tilde{\mathbf{p}}(p)} = \frac{2}{\sigma^2} \left(\mathbf{I}_{K-1} \otimes \tilde{\mathbf{F}}(p) \right) \tilde{\mathbf{H}}(p) \quad (53)$$

$$\boldsymbol{\Upsilon} = \begin{bmatrix} \mathbf{f}_1(1) & \dots & \mathbf{f}_M(1) \\ \vdots & \ddots & \vdots \\ \mathbf{f}_1(P) & \dots & \mathbf{f}_M(P) \end{bmatrix} \in \mathbb{C}^{PN_s \times M} \quad (54)$$

$$\mathbf{G}(p) = \begin{bmatrix} \mathbf{h}_{1,1}(p) & \dots & \mathbf{h}_{1,M}(p) \\ \vdots & \ddots & \vdots \\ \mathbf{h}_{K,1}(p) & \dots & \mathbf{h}_{K,M}(p) \end{bmatrix} \in \mathbb{C}^{KN_s \times M} \quad (55)$$

$$\text{FIM} = \left[\begin{array}{ccc|ccc} \mathbf{J}_{\boldsymbol{\alpha}_2, \boldsymbol{\alpha}_2} & & 0 & & & \\ & \ddots & & \mathbf{J}_{\boldsymbol{\alpha}, \tilde{\mathbf{p}}(2)} & \dots & \mathbf{J}_{\boldsymbol{\alpha}, \tilde{\mathbf{p}}(P)} \\ 0 & & \mathbf{J}_{\boldsymbol{\alpha}_K, \boldsymbol{\alpha}_K} & & & \\ \hline & \mathbf{J}_{\boldsymbol{\alpha}, \tilde{\mathbf{p}}(2)}^T & & \mathbf{J}_{\tilde{\mathbf{p}}(2), \tilde{\mathbf{p}}(2)} & & 0 \\ & \vdots & & & \ddots & \\ & \mathbf{J}_{\boldsymbol{\alpha}, \tilde{\mathbf{p}}(P)}^T & & 0 & & \mathbf{J}_{\tilde{\mathbf{p}}(P), \tilde{\mathbf{p}}(P)} \end{array} \right] \quad (50)$$

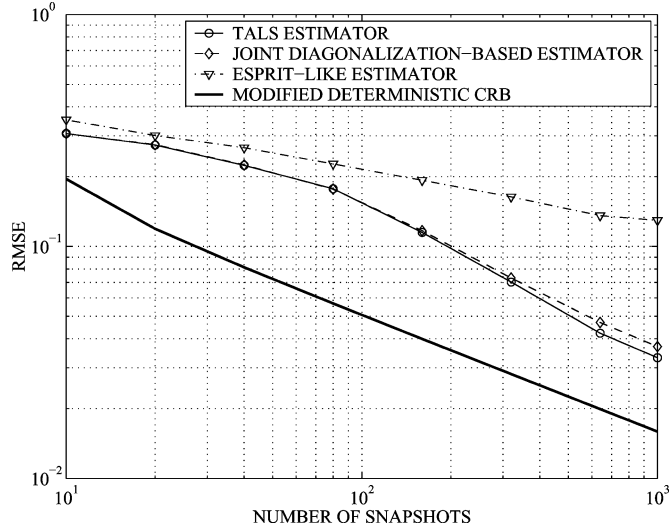


Fig. 1. RMSEs versus N for $K = 10$ and $\text{SNR} = 10$ dB. First example, synchronized users.

$$\tilde{\mathbf{F}}(p) = \begin{bmatrix} \text{Re}\{\mathbf{F}^H(p)\} & -\text{Im}\{\mathbf{F}^H(p)\} \\ \text{Im}\{\mathbf{F}^H(p)\} & \text{Re}\{\mathbf{F}^H(p)\} \end{bmatrix} \quad (56)$$

$$\mathbf{F}(p) = [\mathbf{f}_1(p), \dots, \mathbf{f}_M(p)] \in \mathbb{C}^{N_s \times M} \quad (57)$$

$$\tilde{\mathbf{H}}(p) = [\tilde{\mathbf{H}}_1^T(p), \dots, \tilde{\mathbf{H}}_K^T(p)]^T \quad (58)$$

$$\tilde{\mathbf{H}}_k(p) = \begin{bmatrix} \text{Re}\{\mathbf{H}_k(p)\} \\ \text{Im}\{\mathbf{H}_k(p)\} \end{bmatrix} \quad (59)$$

$$\mathbf{H}_k(p) = [\mathbf{h}_{k,1}(p), \dots, \mathbf{h}_{k,M}(p)] \in \mathbb{C}^{N_s \times M} \quad (60)$$

$$\mathbf{f}_m(p) = \begin{bmatrix} \sqrt{\nu_m(p)} \tilde{s}_m((p-1)N_s + 1), \\ \dots, \sqrt{\nu_m(p)} \tilde{s}_m(pN_s) \end{bmatrix}^T \in \mathbb{C}^{N_s \times 1} \quad (61)$$

$$\mathbf{h}_{k,m}(p) = \begin{bmatrix} \frac{a_{k,m} \tilde{s}_m((p-1)N_s + 1)}{2\sqrt{\nu_m(p)}} \\ \dots, \frac{a_{k,m} \tilde{s}_m(pN_s)}{2\sqrt{\nu_m(p)}} \end{bmatrix}^T \in \mathbb{C}^{N_s \times 1} \quad (62)$$

and \otimes denotes the Kronecker product.

The $(K-1)M \times (K-1)M$ spatial signature-related block of the CRB matrix is given in closed form as

$$\text{CRB}_{\alpha,\alpha} = \left[\mathbf{J}_{\alpha,\alpha} - \frac{2}{\sigma^2} \sum_{p=2}^P (\mathbf{I}_{K-1} \otimes \tilde{\mathbf{F}}(p)) \tilde{\mathbf{H}}(p) \cdot \left[\text{Re}\{\mathbf{G}^H(p)\mathbf{G}(p)\} \right]^{-1} \tilde{\mathbf{H}}^H(p) (\mathbf{I}_{K-1} \otimes \tilde{\mathbf{F}}(p))^H \right]^{-1} \quad (63)$$

where the upper-left block of (50) can be expressed as

$$\mathbf{J}_{\alpha,\alpha} = \begin{bmatrix} \mathbf{J}_{\alpha_2,\alpha_2} & & 0 \\ & \ddots & \\ 0 & & \mathbf{J}_{\alpha_K,\alpha_K} \end{bmatrix} = \frac{2}{\sigma^2} \mathbf{I}_{K-1} \otimes \begin{bmatrix} \text{Re}\{\mathbf{\Upsilon}^H \mathbf{\Upsilon}\} & -\text{Im}\{\mathbf{\Upsilon}^H \mathbf{\Upsilon}\} \\ \text{Im}\{\mathbf{\Upsilon}^H \mathbf{\Upsilon}\} & \text{Re}\{\mathbf{\Upsilon}^H \mathbf{\Upsilon}\} \end{bmatrix}. \quad (64)$$

Proof: See the Appendix.

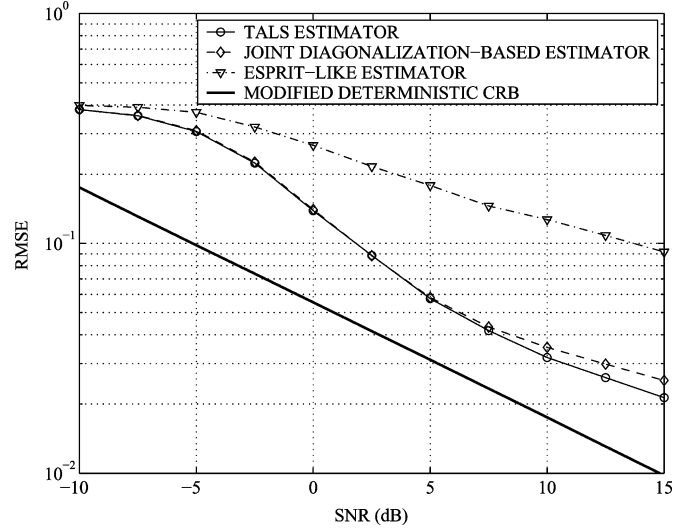


Fig. 2. RMSEs versus the SNR for $K = 10$ and $N = 1000$. First example, synchronized users.

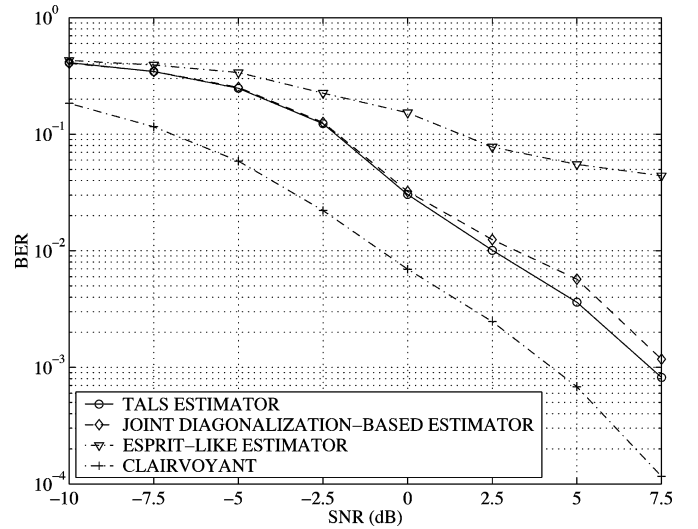


Fig. 3. BERs versus the SNR for $K = 10$ and $N = 1000$. First example, synchronized users.

The obtained CRB expressions will be compared with the performance of the TALS and joint diagonalization-based estimators in the next section.

VII. SIMULATIONS

In this section, the performance of the developed blind spatial signature estimators is compared with that of the ESPRIT-like estimator of [8], the generalized array manifold (GAM) MUSIC estimator of [5], and the derived modified deterministic CRB.

Although the proposed blind estimators are applicable to general array geometries, the ESPRIT-like estimator is based on the uniform linear array (ULA) assumption. Therefore, to compare the estimators in a proper way, we assume a ULA of K omnidirectional sensors spaced half a wavelength apart and $M = 2$ binary phase shift keying (BPSK) user signals impinging on the array from the angles θ_1 and θ_2 relative to the broadside, where in each simulation run, θ_1 and θ_2 are randomly uniformly

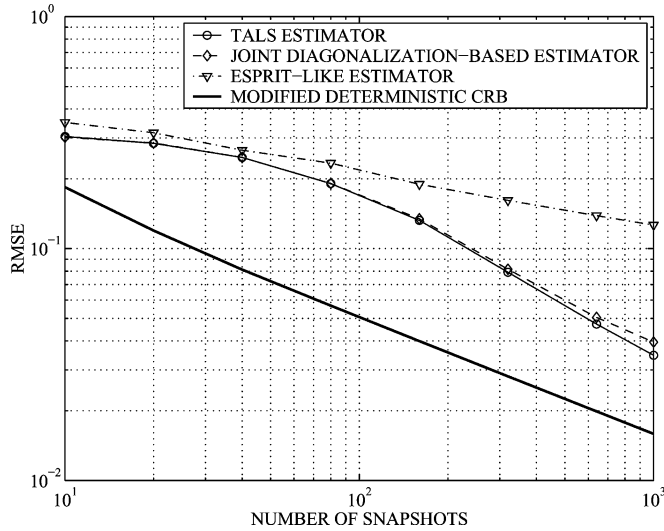


Fig. 4. RMSEs versus N for $K = 10$ and $\text{SNR} = 10$ dB. First example, unsynchronized users.

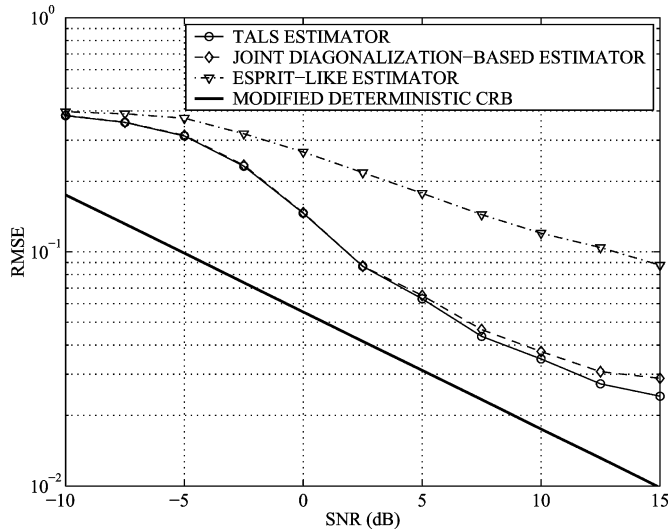


Fig. 5. RMSEs versus the SNR for $K = 10$ and $N = 1000$. First example, unsynchronized users.

drawn from the whole field of view $[-90^\circ, 90^\circ]$. Throughout the simulations, the users are assumed to be synchronized (except Figs. 4 and 5, where the case of unsynchronized users is considered), $P = 10$ subblocks are used in our techniques (except Fig. 10, where P is varied), and the user powers are changed between different subblocks uniformly with a constant power change factor (PCF) of 1.2 (except Fig. 9, where the PCF is varied). Note that $\mathbf{P} = \text{SNR}(\mathbf{E} + \text{PCF} \cdot \mathbf{D})$, where SNR is the average user SNR in a single sensor, \mathbf{E} is the matrix whose elements are all equal to one, \mathbf{D} is a random matrix whose elements are uniformly and independently drawn from the interval $[-0.5, 0.5]$, and it is assumed that $\sigma^2 = 1$.

To implement the PARAFAC TALS and joint diagonalization-based estimators, we use the COMFAC algorithm of [30] and AC-DC algorithm of [32], respectively. Throughout the simulations, both algorithms are initialized randomly. The stopping criterion of the TALS algorithm is the relative improvement in fit from one iteration to the next. The stopping criterion of the

joint diagonalization algorithm is the relative improvement in joint diagonalization error. The algorithms are stopped if such errors become small. Typically, both algorithms converged in less than 30 iterations.

In most figures, the estimator performances are compared in terms of the root-mean-square error (RMSE)

$$\text{RMSE} = \sqrt{\frac{1}{LMK} \sum_{l=1}^L \|\hat{\mathbf{A}}(l) - \mathbf{A}\|_F^2} \quad (65)$$

where $L = 500$ is the number of independent simulation runs, and $\hat{\mathbf{A}}(l)$ is the estimate of \mathbf{A} obtained from the l th run. Note that permutation and scaling of columns is fixed by means of a least-squares ordering and normalization of the columns of $\hat{\mathbf{A}}(l)$. A greedy least-squares algorithm [21] is used to match the (normalized) columns of $\hat{\mathbf{A}}$ to those of \mathbf{A} . We first form an $M \times M$ distance matrix whose (m, n) th element contains the Euclidean distance between the m th column of \mathbf{A} and the n th column of $\hat{\mathbf{A}}$. The smallest element of this distance matrix determines the first match, and the respective row and column of this matrix are deleted. The process is then repeated with the reduced-size distance matrix.

The CRB is averaged over simulation runs as well.

To verify that the RMSE is a proper performance measure in applications to communications problems, one of our figures also illustrates the performance in terms of the BER when the estimated spatial signatures are used together with a typical detection strategy to estimate the transmitted bits.

Example 1—Unknown Sensor Gains and Phases: Following [8], we assume in our first example that the array gains and phases are unknown, i.e., the received data are modeled as (2) with

$$\mathbf{A} = \mathbf{\Gamma} \mathbf{A}_0$$

where \mathbf{A}_0 is the matrix of nominal (plane-wavefront) user spatial signatures, and $\mathbf{\Gamma}$ is the diagonal matrix containing the array unknown gains and phases, i.e., $\mathbf{\Gamma}(\boldsymbol{\gamma}) = \text{diag}\{g_1 e^{j\phi_1}, \dots, g_K e^{j\phi_K}\}$. The unknown gains g_1, \dots, g_K are independently drawn in each simulation run from the uniform random generator with the mean equal to $\sqrt{3}$ and standard deviation equal to one, whereas the unknown phases ϕ_1, \dots, ϕ_K are independently and uniformly drawn from the interval $[0, 2\pi)$.

Fig. 1 displays the RMSEs of our estimators and the ESPRIT-like estimator of [8] along with the CRB versus N for $K = 10$, and $\text{SNR} = 10$ dB. Fig. 2 shows the performances of the same estimators and the CRB versus the SNR for $K = 10$ and $N = 1000$.

Fig. 3 illustrates the performance in terms of the BER when the estimated spatial signatures are used to detect the transmitted bits via the zero-forcing (ZF) detector given by $\text{sign}(\hat{\mathbf{A}}^\dagger \mathbf{y}(n))$. To avoid errors in computing the pseudoinverse of the matrix \mathbf{A} , the runs in which $\hat{\mathbf{A}}^H \hat{\mathbf{A}}$ was ill-conditioned have been dropped. The resulting BERs are displayed versus the SNR for $K = 10$ and $N = 1000$. Additionally, the results of the so-called *clairvoyant* ZF detector $\text{sign}(\mathbf{A}^\dagger \mathbf{y}(n))$ are displayed in this figure. Note that the latter detector corresponds to the ideal case when the source spatial signatures are exactly known, and therefore,

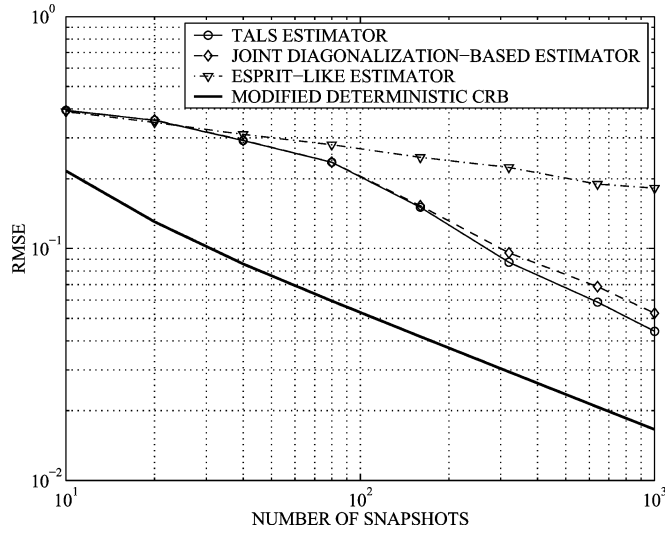


Fig. 6. RMSEs versus N for $K = 4$ and $\text{SNR} = 10$ dB. First example, synchronized users.

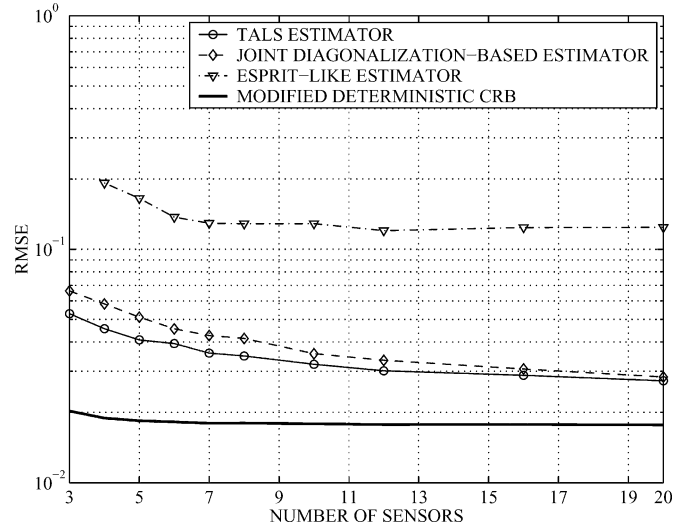


Fig. 8. RMSEs versus K for $\text{SNR} = 10$ dB and $N = 1000$. First example, synchronized users.

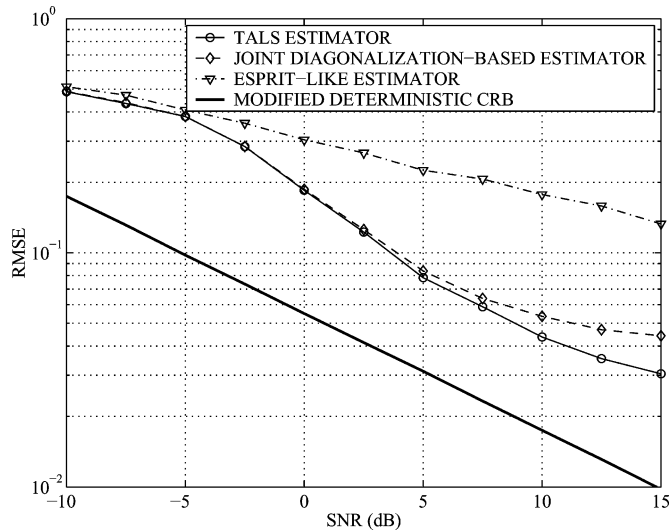


Fig. 7. RMSEs versus the SNR for $K = 4$ and $N = 1000$. First example, synchronized users.

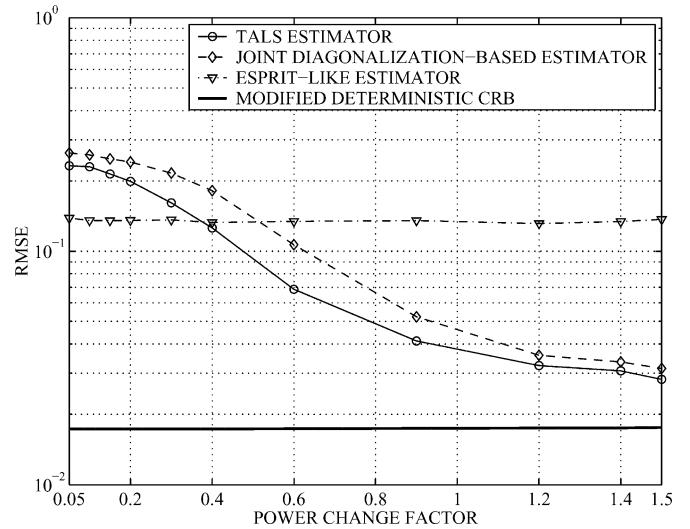


Fig. 9. RMSEs versus the PCF for $\text{SNR} = 10$ dB and $N = 1000$. First example, synchronized users.

it does not correspond to any practical situation. However, its performance is included in Fig. 3 for the sake of comparison as a benchmark.

To demonstrate that the proposed techniques are insensitive to user synchronization, Figs. 4 and 5 show the RMSEs of the same methods and in the same scenarios as in Figs. 1 and 2, respectively, but for the case of unsynchronized users.⁷

To evaluate the performance with a smaller number of sensors, Fig. 6 compares the RMSEs of the estimators tested versus N for $K = 4$ and $\text{SNR} = 10$ dB. Fig. 7 displays the performances of these estimators versus the SNR for $K = 4$ and $N = 1000$.

To illustrate how the performance depends on the number of sensors, the RMSEs of the estimators tested are plotted in Fig. 8 versus K . Figs. 9 and 10 compare the performances of the proposed PARAFAC estimators versus the PCF and the number

⁷That is, the user powers vary without any synchronization between the users.

of subblocks P , respectively. In these figures, $N = 1000$ and $\text{SNR} = 10$ dB.

Example 2—Unknown Coherent Local Scattering: In our second example, we address the scenario where the spatial signature of each nominal (plane-wavefront) user is distorted by local scattering effects [17], [18]. Following [35], the m th user spatial signature is formed in this example by five signal paths of the same amplitude including the single direct path and four coherently scattered paths. Each of these paths is characterized by its own angle and phase. The angle of the direct path is equal to the nominal user DOA, whereas the angles of scattered paths are independently drawn in each simulation run from a uniform random generator with the mean equal to the nominal user DOA and the standard deviations equal to 8° and 10° for the first and second users, respectively. The path phases for each user are uniformly and independently drawn in each simulation run from the interval $[0, 2\pi)$.

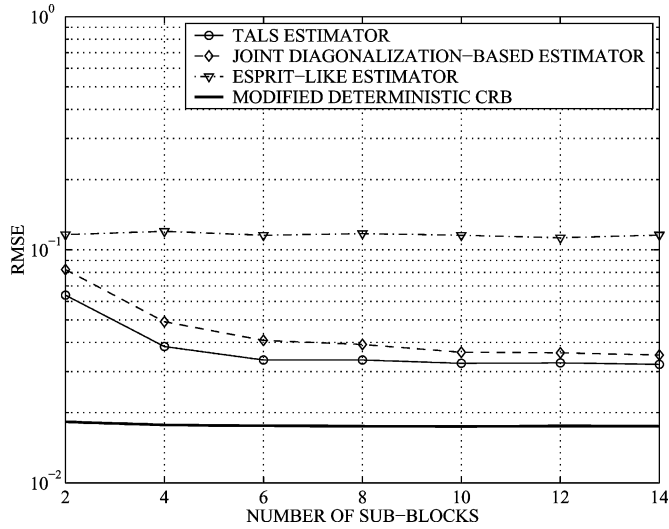


Fig. 10. RMSEs versus P for $\text{SNR} = 10$ dB and $N = 1000$. First example, synchronized users.

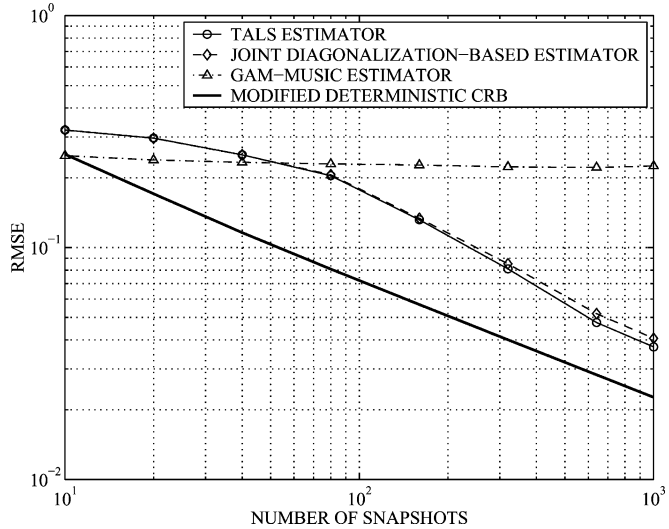


Fig. 11. RMSEs versus N for $K = 10$ and $\text{SNR} = 10$ dB. Second example, synchronized users.

Note that in the second example, it is improper to compare the proposed techniques with the ESPRIT-like estimator of [8] because the latter estimator is not a relevant technique for the scenario considered. Therefore, in this example, we compare our techniques to the GAM-MUSIC estimator of [5].

Fig. 11 displays the performance of the spatial signature estimators tested versus the number of snapshots N for $K = 10$ and $\text{SNR} = 10$ dB. Note that the SNR is defined here by taking into account all signal paths. The performance of the same methods versus the SNR for $K = 10$ and $N = 1000$ is displayed in Fig. 12.

Discussion: Our simulation results clearly demonstrate that the proposed blind PARAFAC spatial signature estimators substantially outperform the ESPRIT-like estimator and the GAM-MUSIC estimator. These improvements are especially pronounced at high values of SNR , number of snapshots, and number of sensors.

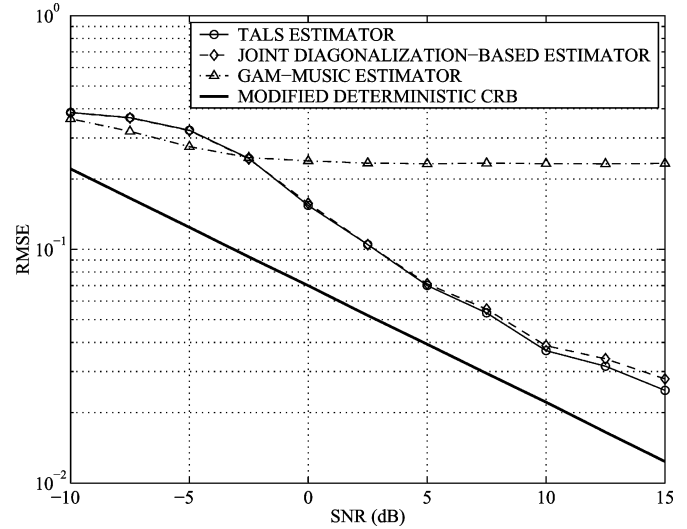


Fig. 12. RMSEs versus the SNR for $K = 10$ and $N = 1000$. Second example, synchronized users.

Comparing Figs. 1 and 2 with Figs. 4 and 5, respectively, we observe that the requirement of user synchronization is not critical to the performance of both the TALS and joint diagonalization-based algorithms. As a matter of fact, the performances of these techniques do not differ much in the cases of synchronized and unsynchronized users. This means that our techniques can easily accommodate intercell interference, provided that out-of-cell users also play up and down their powers, because the fact that out-of-cell users will not be synchronized is not critical performance-wise.

From Fig. 9, it is clear that the performance of the proposed techniques can be improved by increasing the PCF. This figure clarifies that the performance improvements of our estimators over the ESPRIT-like estimator are achieved by means of using the power loading proposed. From Fig. 9, it follows that even moderate values of PCF (1.2...1.4) are sufficient to guarantee that the performances of the proposed PARAFAC estimators are comparable with the CRB and are substantially better than that of the ESPRIT-like estimator.

From Fig. 10, we can observe that the performance of the proposed PARAFAC estimators is also improved when increasing the number of subblocks while keeping the total block length fixed. However, this is only true for small numbers of P ; for $P \geq 8$, curves saturate. Note that this figure makes it clear that even a moderate number of subblocks ($P = 4 \dots 6$) is sufficient to guarantee that the performance is comparable with the CRB and is better than that of the ESPRIT-like estimator. We stress that the effects of the PCF and P cannot be seen from the CRB in Figs. 9 and 10 because the time-averaged user powers and the total number of snapshots do not change in these figures.

Figs. 11 and 12 show that both the TALS and joint-diagonalization based estimators substantially outperform the GAM-MUSIC estimator if the values N and SNR are sufficiently high. Interestingly, the performance of GAM-MUSIC does not improve much when increasing N or SNR . This observation can be explained by the fact that the GAM-MUSIC estimator is biased. Note that from Fig. 11, it follows that GAM-MUSIC may

perform better than the proposed PARAFAC estimators in the case when N is small because the power loading approach does not work properly if there are only a few snapshots per subblock (in this case, the covariance matrix estimates for each subblock become very poor).

Interestingly, as it follows from Fig. 3, the proposed PARAFAC-based techniques combined with the zero forcing (ZF) detector have the same BER slope as the clairvoyant ZF detector, whereas the performance losses with respect to the latter detector do not exceed 3 dB at high SNRs.

There are several reasons why the proposed techniques perform better than the ESPRIT-like algorithm. First of all, even in the case when the array is fully calibrated, the performance of ESPRIT is poorer than that of MUSIC and/or maximum likelihood (ML) estimator because ESPRIT does not take advantage of the full array manifold but only of the array shift-invariance property. Second, our algorithm takes advantage of the user power loading, whereas the ESPRIT-like algorithm does not.

As far as the comparison GAM-MUSIC method is concerned, better performances of the proposed techniques can be explained by the above-mentioned fact that GAM-MUSIC uses the first-order Taylor series approximation, which is only adequate for asymptotically small angular spreads. As a result, the GAM-MUSIC estimator is biased. In addition, similarly to the ESPRIT-like algorithm, GAM-MUSIC does not take any advantage of the user power loading.

Although the performances of the proposed estimators can be made comparable to the CRB with proper choice of PCF and system parameters, they do not attain the CRB. This can be partially attributed to the fact that the modified CRB is an optimistic one in that it assumes knowledge of the temporal source signals, which are unavailable to the blind estimation algorithms. Furthermore, the TALS estimator does not exploit the symmetry of the model ($\mathbf{B} = \mathbf{A}^H$), whereas joint diagonalization relies on an approximate prewhitening step. Both methods rely on finite-sample covariance and noise-power estimates. This explains the observation that the CRB cannot be attained.

VIII. CONCLUSIONS

The problem of blind user spatial signature estimation using the PARAFAC analysis model has been addressed. A time-varying user power loading in the uplink mode has been proposed to make the model identifiable and to enable the application of the PARAFAC analysis model. Identifiability issues and the relevant modified deterministic CRB have been studied, and two blind spatial signature estimation algorithms have been presented. The first technique is based on the PARAFAC fitting TALS regression, whereas the second one makes use of joint matrix diagonalization. These techniques have been shown to provide better performance than the popular ESPRIT-like and GAM-MUSIC blind estimators and are applicable to a much more general class of scenarios.

APPENDIX PROOF OF THEOREM 3

The (l, k) th element of the FIM is given by [34]

$$\text{FIM}_{l,k} = \frac{2}{\sigma^2} \sum_{p=1}^P \sum_{n=(p-1)N_s+1}^{pN_s} \text{Re} \left(\frac{\partial \boldsymbol{\mu}^H(p, n)}{\partial \theta_l} \frac{\partial \boldsymbol{\mu}(p, n)}{\partial \theta_k} \right). \quad (66)$$

Using (45) along with (66), we have

$$\frac{\partial \boldsymbol{\mu}(p, n)}{\partial \text{Re}\{a_{k,m}\}} = \sqrt{\nu_m(p)} \tilde{s}_m(n) \mathbf{e}_k \quad (67)$$

$$\frac{\partial \boldsymbol{\mu}(p, n)}{\partial \text{Im}\{a_{k,m}\}} = j \sqrt{\nu_m(p)} \tilde{s}_m(n) \mathbf{e}_k \quad (68)$$

$$\frac{\partial \boldsymbol{\mu}(p, n)}{\partial \nu_m(p)} = \left[\frac{a_{1,m} \tilde{s}_m(n)}{2\sqrt{\nu_m(p)}}, \dots, \frac{a_{K,m} \tilde{s}_m(n)}{2\sqrt{\nu_m(p)}} \right]^T \quad (69)$$

where \mathbf{e}_k is the vector containing one in the k th position and zeros elsewhere.

Using (67) and (68) along with (66), we obtain that

$$\begin{aligned} \mathbf{J}_{\text{Re}\{a_{k,m}\}, \text{Re}\{a_{k,l}\}} &= \mathbf{J}_{\text{Im}\{a_{k,m}\}, \text{Im}\{a_{k,l}\}} \\ &= \frac{2}{\sigma^2} \sum_{p=1}^P \sum_{n=(p-1)N_s+1}^{pN_s} \text{Re} \left\{ \sqrt{\nu_m(p)\nu_l(p)} \cdot \tilde{s}_m^*(n) \tilde{s}_l(n) \right\} \\ &= \frac{2}{\sigma^2} \text{Re} \left\{ \boldsymbol{\xi}_m^H \boldsymbol{\xi}_l \right\} \end{aligned} \quad (70)$$

where

$$\boldsymbol{\xi}_m \triangleq \left[\mathbf{f}_m^T(1), \dots, \mathbf{f}_m^T(P) \right]^T \in \mathbb{C}^{PN_s \times 1}. \quad (72)$$

Similarly

$$\begin{aligned} \mathbf{J}_{\text{Im}\{a_{k,m}\}, \text{Re}\{a_{k,l}\}} &= -\mathbf{J}_{\text{Re}\{a_{k,m}\}, \text{Im}\{a_{k,l}\}} \\ &= \frac{2}{\sigma^2} \text{Im} \left\{ \boldsymbol{\xi}_m^H \boldsymbol{\xi}_l \right\}. \end{aligned} \quad (73)$$

Therefore

$$\begin{aligned} \mathbf{J}_{\text{Re}\{\boldsymbol{\alpha}_k\}, \text{Re}\{\boldsymbol{\alpha}_k\}} &= \mathbf{J}_{\text{Im}\{\boldsymbol{\alpha}_k\}, \text{Im}\{\boldsymbol{\alpha}_k\}} \\ &= \frac{2}{\sigma^2} \begin{bmatrix} \text{Re} \left\{ \boldsymbol{\xi}_1^H \boldsymbol{\xi}_1 \right\} & \dots & \text{Re} \left\{ \boldsymbol{\xi}_1^H \boldsymbol{\xi}_M \right\} \\ \vdots & \ddots & \vdots \\ \text{Re} \left\{ \boldsymbol{\xi}_M^H \boldsymbol{\xi}_1 \right\} & \dots & \text{Re} \left\{ \boldsymbol{\xi}_M^H \boldsymbol{\xi}_M \right\} \end{bmatrix} \\ &= \frac{2}{\sigma^2} \text{Re} \left\{ \boldsymbol{\Upsilon}^H \boldsymbol{\Upsilon} \right\} \end{aligned} \quad (74)$$

and

$$\begin{aligned} \mathbf{J}_{\text{Im}\{\alpha_k\}, \text{Re}\{\alpha_k\}} &= -\mathbf{J}_{\text{Re}\{\alpha_k\}, \text{Im}\{\alpha_k\}} \\ &= \frac{2}{\sigma^2} \begin{bmatrix} \text{Im}\{\xi_1^H \xi_1\} & \dots & \text{Im}\{\xi_1^H \xi_M\} \\ \vdots & \ddots & \vdots \\ \text{Im}\{\xi_M^H \xi_1\} & \dots & \text{Im}\{\xi_M^H \xi_M\} \end{bmatrix} \\ &= \frac{2}{\sigma^2} \text{Im}\{\mathbf{\Upsilon}^H \mathbf{\Upsilon}\} \end{aligned} \quad (75)$$

Using (74) and (75), we obtain (51). Note that the right-hand side of (51) does not depend on the index k . Hence

$$\begin{aligned} \mathbf{J}_{\alpha, \alpha} &= \begin{bmatrix} \mathbf{J}_{\alpha_2, \alpha_2} & & 0 \\ & \ddots & \\ 0 & & \mathbf{J}_{\alpha_K, \alpha_K} \end{bmatrix} \\ &= \frac{2}{\sigma^2} \mathbf{I}_{K-1} \otimes \begin{bmatrix} \text{Re}\{\mathbf{\Upsilon}^H \mathbf{\Upsilon}\} & -\text{Im}\{\mathbf{\Upsilon}^H \mathbf{\Upsilon}\} \\ \text{Im}\{\mathbf{\Upsilon}^H \mathbf{\Upsilon}\} & \text{Re}\{\mathbf{\Upsilon}^H \mathbf{\Upsilon}\} \end{bmatrix}. \end{aligned} \quad (76)$$

Next, using (69) along with (66), we can write, for $p = 2, \dots, P$ and $m, l = 1, \dots, M$

$$\begin{aligned} [\mathbf{J}_{\tilde{\mathbf{p}}(p), \tilde{\mathbf{p}}(p)}]_{m,l} &= \frac{2}{\sigma^2} \sum_{n=(p-1)N_s+1}^{pN_s} \sum_{k=1}^K \\ &\quad \text{Re} \left\{ \frac{a_{k,m}^* \tilde{s}_m^*(n) a_{k,l} \tilde{s}_l(n)}{4\sqrt{\nu_m(p)\nu_l(p)}} \right\} \\ &= \frac{2}{\sigma^2} \text{Re} \{ \mathbf{c}_m^H(p) \mathbf{c}_l(p) \} \end{aligned} \quad (77)$$

where

$$\mathbf{c}_m(p) \triangleq [\mathbf{h}_{1,m}^T(p), \dots, \mathbf{h}_{K,m}^T(p)]^T \in \mathbb{C}^{KN_s \times 1}. \quad (78)$$

Stacking all M^2 elements given by (77) in one matrix, we have

$$\begin{aligned} \mathbf{J}_{\tilde{\mathbf{p}}(p), \tilde{\mathbf{p}}(p)} &= \frac{2}{\sigma^2} \begin{bmatrix} \text{Re}\{\mathbf{c}_1^H(p)\mathbf{c}_1(p)\} & \dots & \text{Re}\{\mathbf{c}_1^H(p)\mathbf{c}_M(p)\} \\ \vdots & \ddots & \vdots \\ \text{Re}\{\mathbf{c}_M^H(p)\mathbf{c}_1(p)\} & \dots & \text{Re}\{\mathbf{c}_M^H(p)\mathbf{c}_M(p)\} \end{bmatrix} \\ &= \frac{2}{\sigma^2} \text{Re} \{ \mathbf{G}^H(p) \mathbf{G}(p) \}, \quad p = 2, \dots, P. \end{aligned} \quad (79)$$

Finally, using (67)–(69) along with (66), we can write for $p = 2, \dots, P$; $k = 2, \dots, K$ and $m, l = 1, \dots, M$

$$\begin{aligned} [\mathbf{J}_{\text{Re}\{\alpha_k\}, \tilde{\mathbf{p}}(p)}]_{m,l} &= \frac{2}{\sigma^2} \sum_{n=(p-1)N_s+1}^{pN_s} \text{Re} \left\{ \frac{1}{2} \frac{\sqrt{\nu_m(p)}}{\sqrt{\nu_l(p)}} \tilde{s}_m^*(n) a_{k,l} \tilde{s}_l(n) \right\} \\ &= \frac{2}{\sigma^2} \text{Re} \{ \mathbf{f}_m^H(p) \mathbf{h}_{k,l}(p) \} \\ [\mathbf{J}_{\text{Im}\{\alpha_k\}, \tilde{\mathbf{p}}(p)}]_{m,l} &= \frac{2}{\sigma^2} \sum_{n=(p-1)N_s+1}^{pN_s} \text{Re} \left\{ -\frac{j}{2} \frac{\sqrt{\nu_m(p)}}{\sqrt{\nu_l(p)}} \tilde{s}_m^*(n) a_{k,l} \tilde{s}_l(n) \right\} \\ &= \frac{2}{\sigma^2} \text{Im} \{ \mathbf{f}_m^H(p) \mathbf{h}_{k,l}(p) \} \end{aligned}$$

Collecting all $2(K-1)M^2$ elements given by the last two equations in one matrix, we obtain

$$\mathbf{J}_{\alpha, \tilde{\mathbf{p}}(p)} = \frac{2}{\sigma^2} \begin{bmatrix} \begin{bmatrix} \text{Re}\{\mathbf{F}^H(p)\mathbf{H}_2(p)\} \\ \text{Im}\{\mathbf{F}^H(p)\mathbf{H}_2(p)\} \end{bmatrix} \\ \vdots \\ \begin{bmatrix} \text{Re}\{\mathbf{F}^H(p)\mathbf{H}_K(p)\} \\ \text{Im}\{\mathbf{F}^H(p)\mathbf{H}_K(p)\} \end{bmatrix} \end{bmatrix}, \quad p = 2, \dots, P. \quad (80)$$

Observing that

$$\begin{aligned} \begin{bmatrix} \text{Re}\{\mathbf{F}^H(p)\mathbf{H}_k(p)\} \\ \text{Im}\{\mathbf{F}^H(p)\mathbf{H}_k(p)\} \end{bmatrix} &= \begin{bmatrix} \text{Re}\{\mathbf{F}^H(p)\} & -\text{Im}\{\mathbf{F}^H(p)\} \\ \text{Im}\{\mathbf{F}^H(p)\} & \text{Re}\{\mathbf{F}^H(p)\} \end{bmatrix} \\ &\quad \cdot \begin{bmatrix} \text{Re}\{\mathbf{H}_k^H(p)\} \\ \text{Im}\{\mathbf{H}_k^H(p)\} \end{bmatrix} \\ &= \tilde{\mathbf{F}}(p) \tilde{\mathbf{H}}_k(p) \end{aligned} \quad (81)$$

we can further simplify (80) to

$$\mathbf{J}_{\alpha, \tilde{\mathbf{p}}(p)} = \frac{2}{\sigma^2} (\mathbf{I}_{K-1} \otimes \tilde{\mathbf{F}}(p)) \tilde{\mathbf{H}}(p). \quad (82)$$

In addition, note that

$$\mathbf{J}_{\alpha, \tilde{\mathbf{p}}(p)}^T = \mathbf{J}_{\tilde{\mathbf{p}}(p), \alpha}. \quad (83)$$

Using (76), (79), (82), and (83), we obtain the expressions (50)–(62).

Computing the CRB for θ requires the inverse of the $(2(K-1)M + (P-1)M) \times (2(K-1)M + (P-1)M)$ matrix (50). Our objective is to obtain the CRB associated with the vector

parameter α only, avoiding the inverse of the full FIM matrix. Exploiting the fact that the lower right subblock

$$\begin{bmatrix} \mathbf{J}_{\mathbf{p}(2),\mathbf{p}(2)} & & \\ & \ddots & \\ & & \mathbf{J}_{\mathbf{p}(P),\mathbf{p}(P)} \end{bmatrix} \quad (84)$$

of (50) is a block-diagonal matrix and using the partitioned matrix inversion lemma (see [34, p. 572]), after some algebra, we obtain (63) and (64), and the proof is complete.

REFERENCES

- [1] B. Ottersten, "Array processing for wireless communications," in *Proc. 8th IEEE Signal Processing Workshop Statistical Signal Array Process.*, Corfu, Greece, Jul. 1996, pp. 466–473.
- [2] A. J. Paulraj and C. B. Papadias, "Space-time processing for wireless communications," *IEEE Signal Process. Mag.*, vol. 14, pp. 49–83, Nov. 1997.
- [3] J. H. Winters, "Smart antennas for wireless systems," *IEEE Pers. Commun. Mag.*, vol. 5, pp. 23–27, Feb. 1998.
- [4] J. H. Winters, J. Salz, and R. D. Gitlin, "The impact of antenna diversity on the capacity of wireless communication systems," *IEEE Trans. Commun.*, vol. 42, pp. 1740–1751, Feb.–Apr. 1994.
- [5] D. Asztely, B. Ottersten, and A. L. Swindlehurst, "Generalized array manifold model for wireless communication channel with local scattering," *Proc. Inst. Elect. Eng., Radar, Sonar Navigat.*, vol. 145, pp. 51–57, Feb. 1998.
- [6] A. L. Swindlehurst, "Time delay and spatial signature estimation using known asynchronous signals," *IEEE Trans. Signal Process.*, vol. 46, no. 2, pp. 449–462, Feb. 1998.
- [7] S. S. Jeng, H. P. Lin, G. Xu, and W. J. Vogel, "Measurements of spatial signature of an antenna array," in *Proc. PIMRC*, vol. 2, Toronto, ON, Canada, Sep. 1995, pp. 669–672.
- [8] D. Astely, A. L. Swindlehurst, and B. Ottersten, "Spatial signature estimation for uniform linear arrays with unknown receiver gains and phases," *IEEE Trans. Signal Process.*, vol. 47, no. 8, pp. 2128–2138, Aug. 1999.
- [9] A. J. Weiss and B. Friedlander, "Almost blind steering vector estimation using second-order moments," *IEEE Trans. Signal Process.*, vol. 44, no. 4, pp. 1024–1027, Apr. 1996.
- [10] B. G. Agee, S. V. Schell, and W. A. Gardner, "Spectral self-coherence restoral: a new approach to blind adaptive signal extraction using antenna arrays," *Proc. IEEE*, vol. 78, no. 4, pp. 753–767, Apr. 1990.
- [11] Q. Wu and K. M. Wong, "Blind adaptive beamforming for cyclostationary signals," *IEEE Trans. Signal Process.*, vol. 44, no. 11, pp. 2757–2767, Nov. 1996.
- [12] J.-F. Cardoso and A. Souloumiac, "Blind beamforming for non-Gaussian signals," *Proc. Inst. Elect. Eng. F*, vol. 140, no. 6, pp. 362–370, Dec. 1993.
- [13] M. C. Dogan and J. M. Mendel, "Cumulant-based blind optimum beamforming," *IEEE Trans. Aerosp. Electron. Syst.*, vol. 30, pp. 722–741, Jul. 1994.
- [14] E. Gonen and J. M. Mendel, "Applications of cumulants to array processing, Part III: Blind beamforming for coherent signals," *IEEE Trans. Signal Process.*, vol. 45, no. 9, pp. 2252–2264, Sep. 1997.
- [15] A. Belouchrani, K. Abed-Meraim, J.-F. Cardoso, and E. Moulines, "A blind source separation technique using second-order statistics," *IEEE Trans. Signal Process.*, vol. 45, no. 2, pp. 434–444, Feb. 1997.
- [16] N. Yuen and B. Friedlander, "Performance analysis of blind signal copy using fourth order cumulants," *J. Adaptive Contr. Signal Process.*, vol. 10, no. 2/3, pp. 239–266, 1996.
- [17] K. I. Pedersen, P. E. Mogensen, and B. H. Fleury, "A stochastic model of the temporal and azimuthal dispersion seen at the base station in outdoor propagation environments," *IEEE Trans. Veh. Technol.*, vol. 49, no. 2, pp. 437–447, Mar. 2000.
- [18] —, "Spatial channel characteristics in outdoor environments and their impact on BS antenna system performance," in *Proc. Veh. Technol. Conf.*, vol. 2, Ottawa, ON, Canada, May 1998, pp. 719–723.
- [19] R. A. Harshman, "Foundation of the PARAFAC procedure: model and conditions for an "explanatory" multi-mode factor analysis," *UCLA Working Papers Phonetics*, vol. 16, pp. 1–84, Dec. 1970.
- [20] J. B. Kruskal, "Three-way arrays: rank and uniqueness of trilinear decompositions, with application to arithmetic complexity and statistics," *Linear Algebra Applicat.*, vol. 16, pp. 95–138, 1977.
- [21] N. D. Sidiropoulos, G. B. Giannakis, and R. Bro, "Blind PARAFAC receivers for DS-CDMA systems," *IEEE Trans. Signal Process.*, vol. 48, no. 3, pp. 810–823, Mar. 2000.
- [22] N. D. Sidiropoulos and R. Bro, "On the uniqueness of multilinear decomposition of N-way arrays," *J. Chemometr.*, vol. 14, pp. 229–239, 2000.
- [23] N. D. Sidiropoulos, R. Bro, and G. B. Giannakis, "Parallel factor analysis in sensor array processing," *IEEE Trans. Signal Process.*, vol. 48, no. 8, pp. 2377–2388, Aug. 2000.
- [24] M. K. Tsatsanis and C. Kweon, "Blind source separation of nonstationary sources using second-order statistics," in *Proc. 32nd Asilomar Conf. Signals, Syst. Comput.*, vol. 2, Pacific Grove, CA, Nov. 1998, pp. 1574–1578.
- [25] D.-T. Pham and J.-F. Cardoso, "Blind separation of instantaneous mixtures of nonstationary sources," *IEEE Trans. Signal Process.*, vol. 49, no. 9, pp. 1837–1848, Sep. 2001.
- [26] R. L. Harshman, "Determination and proof of minimum uniqueness conditions for PARAFAC1," *UCLA Working Papers Phonetics*, vol. 22, pp. 111–117, 1972.
- [27] J. M. F. ten Berge and N. D. Sidiropoulos, "On uniqueness in CANDECOMP/PARAFAC," *Psychometrika*, vol. 67, no. 3, Sept. 2002.
- [28] J. M. F. ten Berge, N. D. Sidiropoulos, and R. Rocci, "Typical rank and INDSCAL dimensionality for symmetric three-way arrays of order $1 \times 2 \times 2$ or $1 \times 1 \times 3 \times 3$," *Linear Algebra Applicat.*, to be published.
- [29] T. Jiang, N. D. Sidiropoulos, and J. M. F. ten Berge, "Almost sure identifiability of multi-dimensional harmonic retrieval," *IEEE Trans. Signal Process.*, vol. 49, no. 9, pp. 1849–1859, Sep. 2001.
- [30] R. Bro, N. D. Sidiropoulos, and G. B. Giannakis, "A fast least squares algorithm for separating trilinear mixtures," in *Proc. Int. Workshop Independent Component Analysis and Blind Signal Separation*, Aussois, France, Jan. 1999.
- [31] J.-F. Cardoso and A. Souloumiac, "Jacobi angles for simultaneous diagonalization," *SIAM J. Matrix Anal. Applicat.*, vol. 17, pp. 161–164, Jan. 1996.
- [32] A. Yeredor, "Non-orthogonal joint diagonalization in the least-squares sense with application in blind source separation," *IEEE Trans. Signal Process.*, vol. 50, no. 7, pp. 1545–1553, Jul. 2002.
- [33] P. Stoica and A. Nehorai, "Performance study of conditional and unconditional direction-of-arrival estimation," *IEEE Trans. Acoust., Speech, Signal Process.*, vol. 38, no. 10, pp. 1783–1795, Oct. 1990.
- [34] S. M. Kay, *Fundamentals of Statistical Signal Processing: Estimation Theory*. Englewood Cliffs, NJ: Prentice-Hall, 1993.
- [35] S. A. Vorobyov, A. B. Gershman, and Z.-Q. Luo, "Robust adaptive beamforming using worst-case performance optimization: A solution to the signal mismatch problem," *IEEE Trans. Signal Process.*, vol. 51, no. 2, pp. 313–324, Feb. 2003.



Yue Rong (S'03) was born in 1976 in Jiangsu, China. In 1999, he received the Bachelor degrees from Shanghai Jiao Tong University, Shanghai, China, both in electrical and computer engineering. He received the M.Sc. degree in computer science and communication engineering from the University of Duisburg-Essen, Duisburg, Germany, in 2002. Currently, he is working toward the Ph.D. degree at the Department of Communication Systems, University of Duisburg-Essen.

From April 2001 to April 2002, he was a student research assistant at the Fraunhofer Institute of Microelectronic Circuits and Systems. From October 2001 to March 2002, he was with the Application-Specific Integrated Circuit Design Department, Nokia Ltd., Bochum, Germany. His research interests include signal processing for communications, MIMO communication systems, multicarrier communications, statistical and array signal processing, and parallel factor analysis.

Mr. Rong received the Graduate Sponsoring Asia scholarship of DAAD/ABB in 2001.



Sergiy A. Vorobyov (M'02) was born in Ukraine in 1972. He received the M.S. and Ph.D. degrees in systems and control from Kharkiv National University of Radioelectronics (KNUR), Kharkiv, Ukraine, in 1994 and 1997, respectively.

From 1995 to 2000, he was with the Control and Systems Research Laboratory at KNUR, where he became a Senior Research Scientist in 1999. From 1999 to 2001, he was with the Brain Science Institute, RIKEN, Tokyo, Japan, as a Research Scientist. From 2001 to 2003, he was with the Department of Electrical and Computer Engineering, McMaster University, Hamilton, ON, Canada, as a Postdoctoral Fellow. Since 2003, he has been a Research Fellow with the Department of Communication Systems, University of Duisburg-Essen, Duisburg, Germany. He also held short-time visiting appointments at the Institute of Applied Computer Science, Karlsruhe, Germany, and Gerhard-Mercator University, Duisburg. His research interests include control theory, statistical array signal processing, blind source separation, robust adaptive beamforming, and wireless and multicarrier communications.

Dr. Vorobyov was a recipient of the 1996–1998 Young Scientist Fellowship of the Ukrainian Cabinet of Ministers, the 1996 and 1997 Young Scientist Research Grants from the George Soros Foundation, and the 1999 DAAD Fellowship (Germany). He co-received the 2004 IEEE Signal Processing Society Best Paper Award.



Alex B. Gershman (M'97–SM'98) received the Diploma (M.Sc.) and Ph.D. degrees in radiophysics from the Nizhny Novgorod State University, Nizhny Novgorod, Russia, in 1984 and 1990, respectively.

From 1984 to 1989, he was with the Radiotechnical and Radiophysical Institutes, Nizhny Novgorod. From 1989 to 1997, he was with the Institute of Applied Physics, Russian Academy of Science, Nizhny Novgorod, as a Senior Research Scientist. From the summer of 1994 until the beginning of 1995, he was a Visiting Research Fellow at the Swiss Federal Institute of Technology, Lausanne, Switzerland. From 1995 to 1997, he was Alexander von Humboldt Fellow at Ruhr University, Bochum, Germany. From 1997 to 1999, he was a Research Associate at the Department of Electrical Engineering, Ruhr University. In 1999, he joined the Department of Electrical and Computer Engineering, McMaster University, Hamilton, ON, Canada where he is now a Professor. Currently, he also holds a visiting professorship at the Department of Communication Systems, University of Duisburg-Essen, Duisburg, Germany. His research interests are in the area of signal processing and communications, and include statistical and array signal processing, adaptive beamforming, spatial diversity in wireless communications, multiuser and MIMO communications, parameter estimation and detection, and spectral analysis. He has published over 220 technical papers in these areas.

Dr. Gershman was a recipient of the 1993 International Union of Radio Science (URSI) Young Scientist Award, the 1994 Outstanding Young Scientist Presidential Fellowship (Russia), the 1994 Swiss Academy of Engineering Science and Branco Weiss Fellowships (Switzerland), and the 1995–1996 Alexander von Humboldt Fellowship (Germany). He received the 2000 Premier's Research Excellence Award of Ontario and the 2001 Wolfgang Paul Award from the Alexander von Humboldt Foundation, Germany. He is also a recipient of the 2002 Young Explorers Prize from the Canadian Institute for Advanced Research (CIAR), which has honored Canada's top 20 researchers 40 years of age or under. He co-received the 2004 IEEE Signal Processing Society Best Paper Award. He is an Associate Editor of the IEEE TRANSACTIONS ON SIGNAL PROCESSING and the *EURASIP Journal on Wireless Communications and Networking* and a Member of both the Sensor Array and Multichannel Signal Processing (SAM) and Signal Processing Theory and Methods (SPTM) Technical Committees of the IEEE Signal Processing Society. He was Technical Co-Chair of the Third IEEE International Symposium on Signal Processing and Information Technology, Darmstadt, Germany, in December 2003. He is Technical Co-Chair of the Fourth IEEE Workshop on Sensor Array and Multichannel Signal Processing, to be held in Waltham, MA, in July 2006.



Nicholas D. Sidiropoulos (M'92–SM'99) received the Diploma in electrical engineering from the Aristotelian University of Thessaloniki, Thessaloniki, Greece, and the M.S. and Ph.D. degrees in electrical engineering from the University of Maryland, College Park (UMCP), in 1988, 1990 and 1992, respectively.

From 1988 to 1992, he was a Fulbright Fellow and a Research Assistant at the Institute for Systems Research (ISR), UMCP. From September 1992 to June 1994, he served his military service as a Lecturer in the Hellenic Air Force Academy. From October 1993 to June 1994, he also was a member of the technical staff, Systems Integration Division, G-Systems Ltd., Athens, Greece. He was a Postdoctoral Fellow (1994 to 1995) and Research Scientist (1996 to 1997) at ISR-UMCP, an Assistant Professor with the Department of Electrical Engineering, University of Virginia, Charlottesville, from 1997 to 1999, and an Associate Professor with the Department of Electrical and Computer Engineering, University of Minnesota, Minneapolis, from 2000 to 2002. He is currently a Professor with the Telecommunications Division of the Department of Electronic and Computer Engineering, Technical University of Crete, Chania, Crete, Greece, and Adjunct Professor at the University of Minnesota. His current research interests are primarily in signal processing for communications, and multi-way analysis. He is an active consultant for industry in the areas of frequency hopping systems and signal processing for xDSL modems.

Dr. Sidiropoulos is a member of both the Signal Processing for Communications (SPCOM) and Sensor Array and Multichannel Signal Processing (SAM) Technical Committees of the IEEE Signal Processing Society and currently serves as an Associate Editor for the IEEE TRANSACTIONS ON SIGNAL PROCESSING. From 2000 to 2002, he also served as Associate Editor for the IEEE SIGNAL PROCESSING LETTERS. He received the NSF/CAREER award (Signal Processing Systems Program) in June 1998 and an IEEE Signal Processing Society Best Paper Award in 2001.